Morphology and Electronic Structure of Sn-Intercalated TiS_2(0001) Layers

*Junji Yuhara[1], Naoki Isobe[1], Kazuki Nishino[1], Yuya Fujii[1], #Lap Hong Chan[1], Masaaki Araidai[1,2,3], Masashi Nakatake[4]

[1]*Graduate School of Engineering, Nagoya University, Nagoya 464-8603, Japan*

[2]*Institute for Advanced Research, Nagoya University, Nagoya 464-8601, Japan*

[3]*Institute of Materials and Systems for Sustainability, Nagoya University, Nagoya 464-8601, Japan*

[4]*Aichi Synchrotron Radiation Center, Aichi Science & Technology Foundation, Seto, 489-0965, Japan*

ABSTRACT: Surface morphology and electronic structure of layered semiconductor 1-trigonal phase titanium disulfide, i.e. 1T-TiS_2(0001), with Sn intercalation, have been studied by scanning tunneling microscopy (STM), low-energy electron diffraction, synchrotron radiation photoemission spectroscopy, and first-principles calculations based on density functional theory (DFT). From the STM images, we show that Sn atoms are intercalated into TiS_2 layers. The electronic structure exhibits electron Fermi pockets around M points and characteristic band dispersions around the M and K points after Sn intercalation. The DFT calculations reveal the geometrical site of intercalated Sn atom, which is surrounded by six sulfur atoms with D_{3d} symmetry. The calculated electronic band structures are in good agreement with the experimental band structure.

*Corresponding author: Junji Yuhara (j-yuhara@energy.nagoya-u.ac.jp)

#The present affiliation of Lap Hong Chan is National Chung Hsing University, Taichung 40227, Taiwan.

Introduction

The thermoelectric effect has attracted much attention with its sustainable behavior of direct conversion between thermal energy and electrical energy.[1–4] Flexible thermoelectric materials of layered transition metals dichalcogenide (TMD) with intercalations gain more attention and great potential for flexible air-stable n-type thermoelectric.[5] As a TMD material, TiS_2 is a very promising candidate for n-type thermoelectric because of its being environmentally benign, chemical stability, mechanical flexibility, and earth-abundant elements of Ti and S.[5–8]

1-trigonal phase titanium disulfide (1T-TiS_2) has been studied extensively because of its unique 2D character, electronic structure, and highly anisotropic physical properties.[9–11] The 1T-TiS_2 belongs to the group IV transition metal dichalcogenides. It crystallizes in the 1T phase layer structure with octahedral coordination space group trigonal P-3m1 between the transition metal and the chalcogen atoms with the axes of the primitive unit cell of a = 0.3409 nm and c = 0.5685 nm, determined by X-ray diffraction (XRD),[11] forming a layer with three atoms thick and a six-fold symmetry structure of either Ti and S atoms with a lattice spacing of 0.34 nm. The layers are separated by van der Waals gap.

Suga *et al*. have reported Ni intercalated 1T-TiS_2(0001) surface shows a characteristic behavior of the hole pockets examined by momentum spectroscopy with first-principles calculations based on density functional theory (DFT).[12] The hole Fermi surface pocket is suggested from Hall measurement in contrast to M_xTiS_2 with Mn, Fe, and Co.[13] Several experimental studies on transition metal intercalated TiS_2 were compared to theoretical calculations on a self-consistent augmented plane wave or Hartree-Fock methods.[10,14–19] Since TiS_2 has high carrier concentration in the semimetal range, intercalating elements lead to an increase in the carrier performance. The misfit layered compounds, associated with rock salt structure of post-transition metal sulfite, were formed in TiS_2 by charge transferring from

post-transition metal sulfite to TiS_2, which caused a significant reduction in electrical resistivity and thermal conductivity.[20] A series of post-transition metals such as Pb, Bi, and Sn, intercalated into TiS_2 as a misfit layered compound of composition $(MS)_{1+x}(TiS_2)_2$, were investigated by Wan *et al.*, which shows low lattice thermal conductivity close to or even lower than the predicted minimum thermal conductivity. However, the details of the electronic band dispersions are not clarified yet.

Recently, elemental two-dimensional materials have been received great attention. Especially, growth of group 14 elemental honeycomb lattice, such as silicene[21,22], germanene[23,24], stanene[25,26], and plumbene[27], have been studied intensively for its unique electronic structures. They can be promising candidates for the hetero-structure materials together with TMD layered materials. Hence, it is highly desired to examine the group 14 interaction into TiS_2(0001).

In this work, tin has been chosen as intercalation on the layered semiconductor TiS_2(0001) surface to investigate the morphology and electronic structure using scanning tunneling microscope (STM), low-energy electron diffraction (LEED), angle-resolved photoemission spectroscopy (ARPES), along with DFT calculations for the geometry and electronic band structures.

Experimental and Computational methods

The experiments were performed using an ultra-high vacuum (UHV) chamber with STM, LEED, and Auger electron spectroscopy (AES) installed in Nagoya University and an ultra-high vacuum chamber with ARPES installed in the Aichi synchrotron radiation center (AichiSR). Both systems consisted of a preparation chamber with a base pressure of 5×10^{-10} mbar, an analysis chamber with a base of 1×10^{-10} mbar. All STM images presented were

acquired at room temperature (RT) in a constant-current mode with position sample biases between +1.0 V and +2.0 V and tunneling currents of 0.2−0.5 nA. STM tips were prepared by electrochemical etching in a KOH solution of W wire and followed by Ar sputtering. A rear-view LEED-AES optics (Omicron) was operated with a LaB_6 filament. The LEED patterns were examined at incident energy from 50 eV to 150 eV. All apparatus was situated on an air damper with an active vibration isolation system. The system at AichiSR was equipped a 200 mm radius hemispherical photoelectron analyzer with a wide-angle electron lens. The ARPES band mapping near Fermi energy was obtained at the sample temperature of 10 K. The overall resolution was smaller than 30 meV.

A piece of 1*T*-TiS_2 single crystal was bonded between a diameter of 8 mm stainless hat-shape substrate and L-shape stainless plate by a conductive adhesive. The azimuth rotation angles for the specimen for ARPES measurements are pre-checked using LEED pattern and are adjusted by rotating the hat-shape substrate in air. Clean TiS_2 surface was obtained by the standard *in situ* cleavage with removing the *L*-shape stainless plate at a base pressure of the UHV condition. The cleanliness of TiS_2 surface was measured by AES spectra after *in situ* cleavage. Sn was deposited onto the TiS_2 surface at RT in UHV from a well-degassed quartz crucible evaporator operating at a deposition rate of 0.06 monolayer (ML)/min, as measured by a quartz crystal microbalance placing at the sample position. We define one monolayer as an atomic density of a TiS_2 plane of 9.9×10^{14} atoms/cm^2. The deposition rate was accurately calibrated by Rutherford backscattering spectroscopy (RBS). For the RBS measurement, we prepared a graphite substrate with an ultra-thin tin film on the surface. Details of the experimental setup for RBS have been published elsewhere.[28] The errors in the mentioned coverage ratios were less than 5 %. The electronic band structure of TiS_2(0001) layers, that of Sn-intercalated TiS_2 were measured along the Γ−M direction and

around K point with a photon energy of 70 eV.

All the DFT calculations were performed by the VASP (Vienna *ab initio* simulation package) code[29,30] in which wave functions are expanded by plane waves. The projector augmented wave (PAW) method was used to describe the interactions between the ionic core and valence electrons.[31] The vdW-DF2 functional[32] was employed as the exchange-correlation energy functional. For the calculations of Sn intercalated TiS_2(0001) layers, the size of the simulation cell was a = 3.513 Å, b = 3.513 Å and c = 90.0 Å, including a vacuum region larger than 15 Å along the c direction to eliminate artificial interaction between periodic slab images. The TiS_2 substrate was represented by 12 atomic layers slab, with single Sn atom located just below the outermost layer, surrounded by six sulfur atoms with D_{3d} symmetry. The atomic configuration except for the central two layers was relaxed until the forces acting on atoms become smaller than 5 meV/Å. The cutoff energy for the plane-wave basis set used was taken to be 500 eV. The Brillouin zone of the unit cell was sampled with a 10×10×1 gamma-center k-point grid.

Results and discussions

Figure 1 shows the LEED patterns and experimental STM images of clean and Sn-deposited surfaces for 0.1 ML and 0.8 ML. For the clean surface, the wide-scale STM image shows a wide terrace with an atomic step, while a wrinkle and line defect are also randomly detected. Moreover, there is a small particle on the terrace randomly, originating from the intercalated Ti and/or S atoms. The LEED pattern exhibits a three-fold symmetry with a very sharp and bright spot of (1×1) structure, shown as an inset in the STM image. The line profile between A—B as marked in the STM image shows a step height to be 0.55 nm, which is in good agreement with the literature data of monoatomic step height of c-axis oriented TiS_2.[11]

When the Sn atoms for 0.1 ML are deposited onto a clean surface, the terrace exhibits two types of domains, whose step heights are 0.55 nm and 0.8 nm which are estimated from the section profiles along C—D and E—F marked in the STM image. On the higher terraces, small hole defect features with about 1 to 2 nm in diameter appear. These holes are very much similar to the intercalation-induced lattice defects at Na intercalated VSe_2, as reported by *Brauer et al*.[33] If the island grows from the step edge on the terrace, the hole-like features are seldom formed. Therefore, it is determined that Sn atoms dissolve into TiS_2 layers from step edge forming a tin intercalation layer, which induce the step height expansion from 0.55 nm to 0.8 nm. For the LEED pattern, the primitive spots clearly exhibit and no additional spots are observed.

When the amount of Sn deposited increases to 0.8 ML, the area of Sn intercalation increases through sequential filling and widening of the interlayer gaps, starting from the step edges, as well as the growth of three-dimensional (3D) Sn islands in the middle of the terrace, as shown in Figure 1c. The section profiles G—H and I—J indicate that the step heights are estimated to be 0.25 nm and 0.8 nm, respectively. Therefore, the height difference between J and H is 1.05 nm, indicating two-layer intercalations, as shown in the illustration in Figure 1d. The height of the islands is estimated to be 0.4 nm as marked in the STM images with section profile K—L. Since atomic size and interatomic distance in metallic Sn-Sn bond length are 0.15 nm and 0.32 nm, respectively,[34] we considered that the 3D Sn island is composed of two atomic layers. The LEED pattern shows (1×1) spots. The spots intensity becomes weaker and broader in comparison with the clean surface. The LEED pattern shows (1×1) spots. Most of the Sn atoms are intercalated, not on the surface. Since no extra spots are observed, the Sn atoms intercalated do not form a superstructure, except the primitive (1×1) structure identical to TiS_2 unit cell, whose lattice constant is 0.34 nm. Figure 2 shows a simplified representation

of the crystal structure of Sn-intercalated TiS_2(0001) layers.

The clean and Sn-intercalated surfaces were measured by ARPES to examine the electronic structure, as shown in Figure 3. Typical band dispersion for clean TiS_2 surface is shown in Figure 3a along the high-symmetry M-Γ-M direction. The valence band structures are clearly shown at the binding energy below 0.4 eV, while no band structures are observed at the Fermi energy. After the Sn deposition for 0.8 ML, an electron Fermi pocket is recognized around M point, as shown in Figure 3b. The corresponding PES spectra are shown in Figure 3f. It is considered that electron charges transfer from Sn atoms to the TiS_2 conduction band, which is originally located above the Fermi energy, result in the formation of electron pocket just below the Fermi energy. The electron Fermi pockets around M point are already formed after the Sn deposition for 0.1 ML (Figure S1, Supporting information). The characteristic electron Fermi pockets are similar to those observed in the Ni intercalation in TiS_2.[12] While the characteristic hole Fermi pockets are also reported around Γ point in the Ni intercalation,[12] no hole pockets are recognized after Sn intercalation in the present study.

Figure 3c shows an Sn related band dispersion, namely Sn-1, around M point. The Sn-1 band comes down from Γ point and the band shows the lowest energy at 2.3 eV. Moreover, a linear-like band dispersion, namely Sn-2, is clearly seen around the K point, as shown in Figure 3d. The linear-like bands cross at 1.3 eV below Fermi energy. These bands indicate that the intercalated Sn atoms occupy the specific site with a periodicity identical to the TiS_2(0001)(1×1) unit cell. The results are consistent with the LEED patterns showing primitive (1×1) spots after Sn intercalations.

Constant energy maps for the Sn-intercalated TiS_2 surface are shown in Figure 4. The electron Fermi pocket is clearly seen at M points at the Fermi energy level, as shown in Figure 4a. The band dispersion, Sn-1, is recognized as a star-shaped band around Γ point. As

increasing the binding energy, the band shape changes form star-shaped into a hexagonal-like shape, as shown in Figure 4b. The Sn-2 band clearly exhibit a triangle-like shape around the K point. As increasing the binding energy, sizes of the triangle become smaller and smaller and cross at with binding energy of 1.3 eV at K point.

In order to identify the electronic band structure and the geometrical site of Sn atoms intercalated, possible Sn configurations in between 1_{st} and 2_{nd} TiS_2 layers in the (1×1) unit cell, assigned with one or two Sn atoms, have been prepared. The DFT structural optimization for the structural models with two Sn atoms in the (1×1) unit cell exhibit that the distance between 1_{st} and 2_{nd} TiS_2 layers drastically increase after sn intercalations, which is inconsistent with STM height profiles. On the contrary, the structural optimization for single Sn atoms models in the (1×1) unit cell becomes the interlayer distance to be 0.8 nm, consistent with the STM section profiles. Moreover, the Sn-intercalated area is estimated to be about 10 % from the STM images after the Sn deposition for 0.1 ML. Thus, it is considered that there is only one Sn atom in (1×1) unit cell. Furthermore, the number of electronic bands related to Sn atoms become twice in comparison with the band dispersion observed in ARPES. Therefore, it is determined that there is only one Sn atom in between 1_{st} and 2_{nd} TiS_2 layers for (1×1) unit cell.

Figure 5 shows the optimized structural model and calculated band structures. The geometrical site of Sn atom is in between 1_{st} and 2_{nd} layers surrounded by six sulfur atoms with D_{3d} symmetry, as shown in Figures 5a and 5b. The electronic band structure is along M–Γ–M and K–K, shown in Figures 5c and 5d, in accordance with the experimental band dispersion in Figures 3d and 3e. The electron Fermi pocket around M point is well consistent with the experimental band structure. Two kinds of band dispersions, Sn-1 and Sn-2, are also well reproduced, although the binding energy at M and K points are 1.4 and 0.8 eV, which are

significantly lower than the experimental values of 2.3 and 1.3 eV, respectively. The differences are attributed to the exchange-correlation functional, since it is responsible for the shape of band dispersion. Heyd-Scuseria-Ernzerhof functional could be essential to reproduce the detailed electronic structure quantitatively.[35]

Calculated constant energy map at the Fermi energy for the Sn-intercalated TiS_2 surface is shown in Figure 6. The electron Fermi pocket is clearly seen at M points. The star-shaped band is also reproduced, looking like something between star-shape and hexagonal-shape. The triangle-like shaped band structure of Sn-2 is also clearly observed around the K and K' point (Figure S2, Supporting information). These band structures are very much consistent with experimental kx-ky band mapping at the Fermi energy. Therefore, it is concluded that intercalated Sn atoms occupy the site surrounded by six sulfur atoms with D_{3d} symmetry.

The intercalated Ni atoms 1*T*-TiS_2(0001) layers also occupy the site with the D_{3d} symmetry[12]. However, electronic bands, such as Sn-1 and Sn-2, were not observed experimentally. The difference may come from the elemental character between the transition metal and group 14 element with its electronic configuration of *sp* orbitals.

Conclusions

In summary, we examined the morphology and electronic state of Sn deposited 1*T*-TiS_2(0001) surface using combined techniques of STM, LEED, and ARPES, with DFT calculations. The combined techniques revealed Sn intercalations in TiS_2, exhibiting a characteristic electron Fermi pockets. In addition, two kinds of band dispersions, Sn-1 and Sn-2, were observed around M and K points, respectively, which is related to the intercalated Sn atoms confirmed by DFT calculations. For geometrical sites, The intercalated Sn atoms are determined to be surrounded by six sulfur atoms with D_{3d} symmetry.

Acknowledgments

The authors thanks H. Negishi for providing samples of 1*T*-TiS_2(0001). The authors are grateful to Nagoya University Synchrotron Radiation Research Center for financial support for ARPES measurements, which were conducted at the BL7U of Aichi Synchrotron Radiation Center, Aichi Science & Technology Foundation, Aichi, Japan (No.2018001). JY acknowledges financial support from Toyoaki Scholarship Foundation in 2017. MA is partly supported by JSPS KAKENHI Grant Number 19H04541. The computation in this work has been done in part using the facilities at the Information Technology Center, Nagoya University.

References

(1) Snyder, G. J.; Toberer, E. S. Complex Thermoelectric Materials. *Mater. Sustain. ENERGY* **2010**, *7*, 10.

(2) Zhou, Y.; Zhao, L.-D. Promising Thermoelectric Bulk Materials with 2D Structures. *Adv. Mater.* **2017**, *29* (45), 1702676.

(3) Tan, G.; Zhao, L.-D.; Kanatzidis, M. G. Rationally Designing High-Performance Bulk Thermoelectric Materials. *Chem. Rev.* **2016**, *116* (19), 12123–12149.

(4) Zhang, X.; Zhao, L.-D. Thermoelectric Materials: Energy Conversion between Heat and Electricity. *J. Materiomics* **2015**, *1* (2), 92–105.

(5) Wan, C.; Gu, X.; Dang, F.; Itoh, T.; Wang, Y.; Sasaki, H.; Kondo, M.; Koga, K.; Yabuki, K.; Snyder, G. J.; et al. Flexible N-Type Thermoelectric Materials by Organic Intercalation of Layered Transition Metal Dichalcogenide TiS_2. *Nat. Mater.* **2015**, *14* (6), 622–627.

(6) Wan, C.; Kodama, Y.; Kondo, M.; Sasai, R.; Qian, X.; Gu, X.; Koga, K.; Yabuki, K.; Yang, R.; Koumoto, K. Dielectric Mismatch Mediates Carrier Mobility in Organic-Intercalated Layered TiS_2. *Nano Lett.* **2015**, *15* (10), 6302–6308.

(7) Wan, C.; Tian, R.; Azizi, A. B.; Huang, Y.; Wei, Q.; Sasai, R.; Wasusate, S.; Ishida, T.; Koumoto, K. Flexible Thermoelectric Foil for Wearable Energy Harvesting. *Nano Energy* **2016**, *30*, 840–845.

(8) Tian, R.; Wan, C.; Wang, Y.; Wei, Q.; Ishida, T.; Yamamoto, A.; Tsuruta, A.; Shin, W.; Li, S.; Koumoto, K. A Solution-Processed TiS_2/Organic Hybrid Superlattice Film towards Flexible Thermoelectric Devices. *J. Mater. Chem. A* **2017**, *5* (2), 564–570.

(9) Martinez, H.; Auriel, C.; Gonbeau, D.; Loudet, M.; Pfister-Guillouzo, G. Studies of 1T TiS_2 by STM, AFM and XPS: The Mechanism of Hydrolysis in Air. *Appl. Surf. Sci.* **1996**,

93 (3), 231–235.

(10) Chen, C. H.; Fabian, W.; Brown, F. C.; Woo, K. C.; Davies, B.; DeLong, B.; Thompson, A. H. Angle-Resolved Photoemission Studies of the Band Structure of $TiSe_2$ and TiS_2. *Phys. Rev. B* **1980**, *21* (2), 615–624.

(11) Martinez, H.; Azavant, P.; Loudet, M. Interpretation of Scanning Tunneling Microscopy and Atomic Force Microscopy Images of 1T-TiS_2. *Surf. Sci.* **1998**, *400* (1–3), 247–257.

(12) Suga, S.; Tusche, C.; Matsushita, Y.; Ellguth, M.; Irizawa, A.; Kirschner, J. Momentum Microscopy of the Layered Semiconductor TiS_2 and Ni intercalated $Ni_{1/3}TiS_2$. *New J. Phys.* **2015**, *17* (8), 083010.

(13) Negishi, H.; Shoube, A.; Takahashi, H.; Ueda, Y.; Sasaki, M.; Inoue, M. Magnetic Properties of Intercalation Compounds M_xTiS_2 (M = 3*d* Transition Metal). *J. Magn. Magn. Mater.* **1987**, *67* (2), 179–186.

(14) Matsushita, T.; Suga, S.; Kimura, A.; Negishi, H.; Inoue, M. Angle-Resolved Photoemission Study of Ni-Intercalated 1T−TiS_2. *Phys. Rev. B* **1999**, *60* (3), 1678–1686.

(15) Matsushita, T.; Suga, S.; Tanaka, Y.; Shigeoka, H.; Nakatani, T.; Okuda, T.; Terauchi, T.; Shishidou, T.; Kimura, A.; Daimon, H.; et al. Angle-Resolved Photoemission Study of M_xTiS_2 (M=Mn, Fe, Co, Ni; x=1/3, 1/4). *J. Electron Spectrosc. Relat. Phenom.* **1996**, *78*, 477–480.

(16) Scharli, M.; Brunner, J.; Vaterlaus, H. P.; Levy, F. The Influence of V Impurities on the Electronic and Vibrational Properties of TiS_2 Single Crystals. II. Angular-Resolved Photoemission Studies. *J. Phys. C Solid State Phys.* **1983**, *16* (8), 1527.

(17) Suzuki, N.; Yamasaki, T.; Motizuki, K. Electronic Band Structures of Intercalation Compounds of 3*d* Transition Metals with TiS_2. *J. Magn. Magn. Mater.* **1987**, *70* (1), 64–66.

(18) Teshima, T.; Suzuki, N.; Motizuki, K. Electronic Band Structures of 1T-Type TiS_2 Intercalated with Light 3d Transition-Metals. *J. Phys. Soc. Jpn.* **1991**, *60* (3), 1005–1010.

(19) Clerc, D. G.; Poshusta, R. D.; Hess, A. C. Periodic Hartree−Fock Study of Li_xTiS_2, $0 \leq x \leq 1$: The Structural, Elastic, and Electronic Effects of Lithium Intercalation in TiS2. *J. Phys. Chem. A* **1997**, *101* (47), 8926–8931.

(20) Wan, C.; Wang, Y.; Wang, N.; Koumoto, K. Low-Thermal-Conductivity $(MS)_{1+x}(TiS_2)_2$ (M = Pb, Bi, Sn) Misfit Layer Compounds for Bulk Thermoelectric Materials. *Materials* **2010**, *3* (4), 2606–2617.

(21) Vogt, P.; De Padova, P.; Quaresima, C.; Avila, J.; Frantzeskakis, E.; Asensio, M. C.; Resta, A.; Ealet, B.; Le Lay, G. Silicene: Compelling Experimental Evidence for Graphenelike Two-Dimensional Silicon. *Phys. Rev. Lett.* **2012**, *108* (15), 155501.

(22) Fleurence, A.; Friedlein, R.; Ozaki, T.; Kawai, H.; Wang, Y.; Yamada-Takamura, Y. Experimental Evidence for Epitaxial Silicene on Diboride Thin Films. *Phys. Rev. Lett.* **2012**, *108* (24), 245501.

(23) Dávila, M. E.; Xian, L.; Cahangirov, S.; Rubio, A.; Le Lay, G. Germanene: A Novel Two-Dimensional Germanium Allotrope Akin to Graphene and Silicene. *New J. Phys.* **2014**, *16* (9), 095002.

(24) Yuhara, J.; Shimazu, H.; Ito, K.; Ohta, A.; Araidai, M.; Kurosawa, M.; Nakatake, M.; Le Lay, G. Germanene Epitaxial Growth by Segregation through Ag(111) Thin Films on Ge(111). *ACS Nano* **2018**, *12* (11), 11632–11637.

(25) Zhu, F.; Chen, W.; Xu, Y.; Gao, C.; Guan, D.; Liu, C.; Qian, D.; Zhang, S.-C.; Jia, J. Epitaxial Growth of Two-Dimensional Stanene. *Nat. Mater.* **2015**, *14* (10), 1020–1025.

(26) Yuhara, J.; Fujii, Y.; Nishino, K.; Isobe, N.; Nakatake, M.; Xian, L.; Rubio, A.; Le Lay, G. Large Area Planar Stanene Epitaxially Grown on Ag(111). *2D Mater.* **2018**, *5* (2),

025002.

(27) Yuhara, J.; He, B.; Matsunami, N.; Nakatake, M.; Le Lay, G. Graphene's Latest Cousin: Plumbene Epitaxial Growth on a "Nano WaterCube." *Adv. Mater.* **2019**, *31 (27)*, 1901017.

(28) Inoue, M.; Tanaka, S.; Yuhara, J.; Morita, K. Ion Impact Desorption of Metal Atoms from Si(111)-√3×√3-Metal Surfaces. *Nucl. Instrum. Methods Phys. Res. Sect. B Beam Interact. Mater. At.* **1991**, *58* (3), 411–416.

(29) Kresse, G.; Furthmüller, J. Efficient Iterative Schemes for Ab Initio Total-Energy Calculations Using a Plane-Wave Basis Set. *Phys. Rev. B* **1996**, *54* (16), 11169.

(30) Kresse, G.; Joubert, D. From Ultrasoft Pseudopotentials to the Projector Augmented-Wave Method. *Phys. Rev. B* **1999**, *59* (3), 1758.

(31) Blöchl, P. E. Projector Augmented-Wave Method. *Phys. Rev. B* **1994**, *50* (24), 17953–17979.

(32) Lee, K.; Murray, É. D.; Kong, L.; Lundqvist, B. I.; Langreth, D. C. Higher-Accuracy van Der Waals Density Functional. *Phys. Rev. B* **2010**, *82* (8), 081101.

(33) Brauer, H. E.; Ekvall, I.; Olin, H.; Starnberg, H. I.; Wahlström, E.; Hughes, H. P.; Strocov, V. N. Na Intercalation of VSe_2 Studied by Photoemission and Scanning Tunneling Microscopy. *Phys. Rev. B* **1997**, *55* (15), 10022–10026.

(34) Lee, J. A.; Raynor, G. V. The Lattice Spacings of Binary Tin-Rich Alloys. *Proc. Phys. Soc. Sect. B* **1954**, *67* (10), 737–747.

(35) Heyd, J.; Scuseria, G. E.; Ernzerhof, M. Hybrid Functionals Based on a Screened Coulomb Potential. *J. Chem. Phys.* **2003**, *118* (18), 8207–8215.

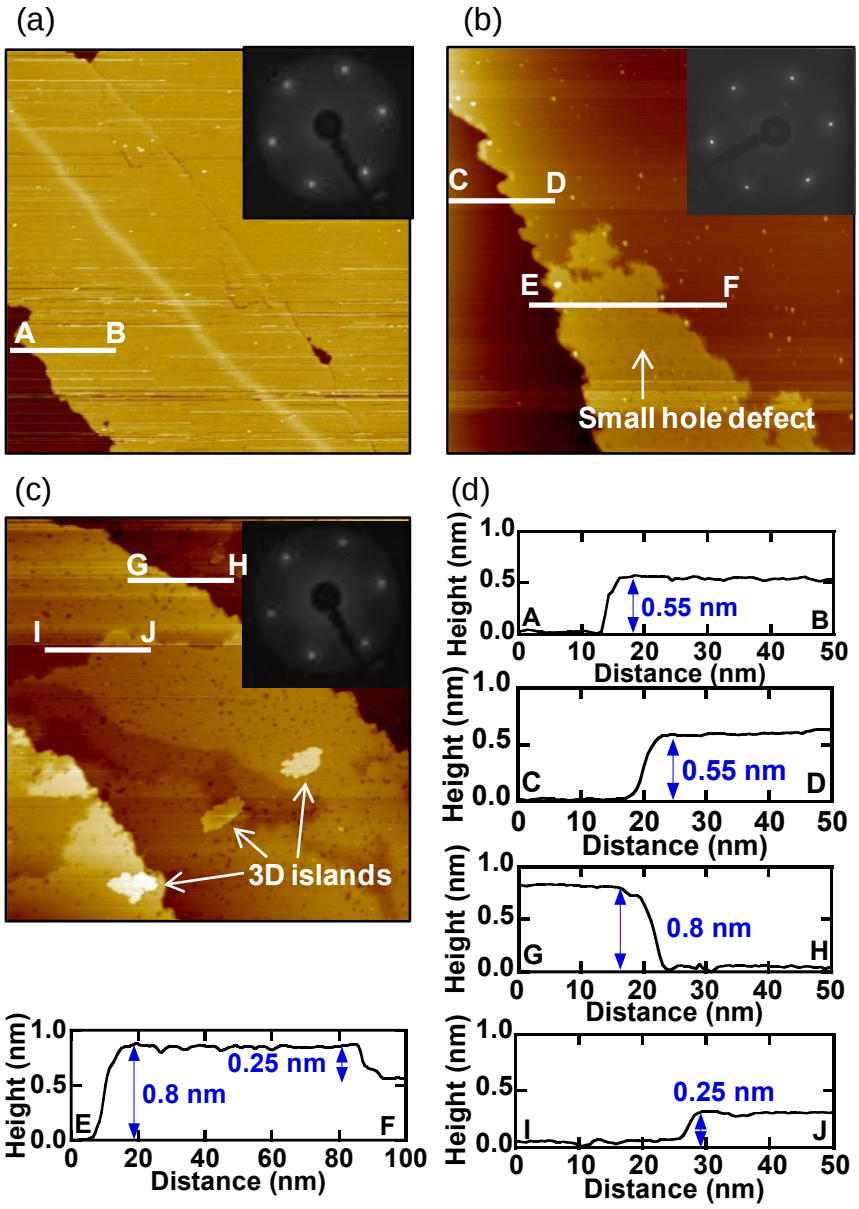

Figure 1. 200 × 200 nm STM images, LEED patterns for (a) clean TiS_2 surface and the Sn-deposited TiS_2 surfaces for (b) 0.1 ML and (c) 0.8 ML. (d) Sectional profiles along the lines as marked in the STM images.

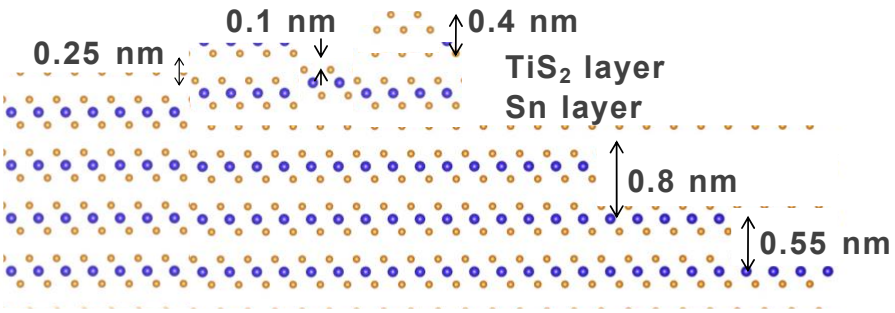

Figure 2. Schematic diagram of the crystal structure of Sn-intercalated TiS_2 layers with a Sn 3D island (side view).

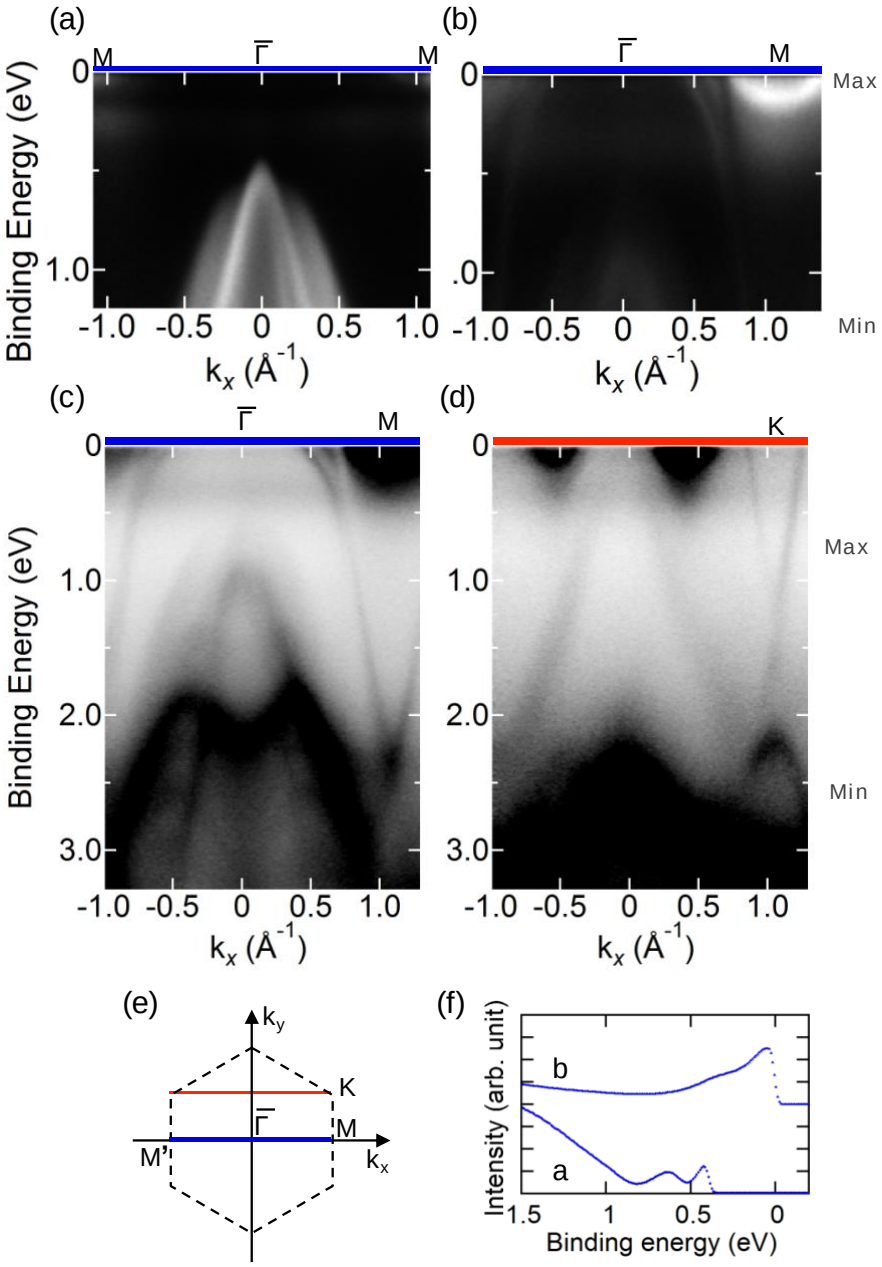

Figure 3. ARPES intensity plots of (a) clean TiS_2(0001) surface and (b) the Sn-intercalated TiS_2 surface for 0.8 ML, measured along M–Γ–M direction. Wide energy ARPES intensity plots for the 0.8 ML Sn-intercalated TiS_2 surface measured along (c) M–$\bar{\Gamma}$–M and (d) K–K. (e) The illustration of relationship of 1st Brillouin zone and horizontal lines of (a) to (d). (f) PES spectra of (a) and (b).

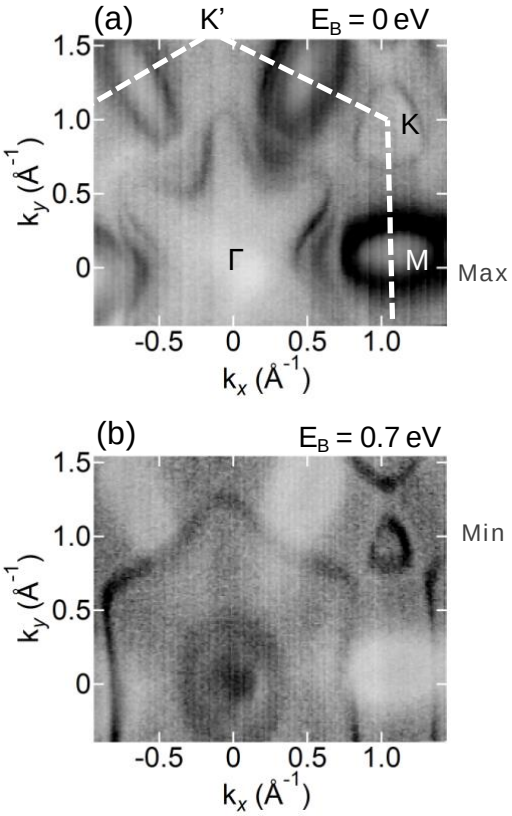

Figure 4. Electronic band structure of the Sn-intercalated TiS_2 for 0.8 ML. Constant energy contour obtained at the binding energies of (a) 0.01 and (b) 0.7 eV, within an interval of ±0.01 eV.

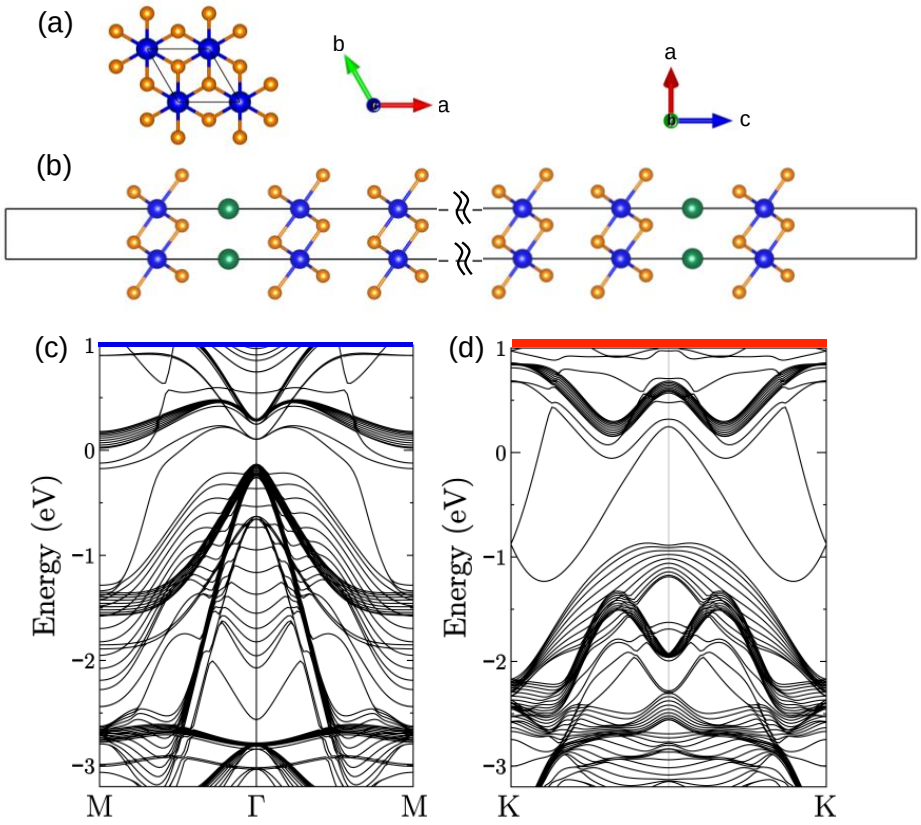

Figure 5. (a) Top view and (b) side view of 1T-TiS_2(0001) slab model consisting of 12 TiS_2 layers with single Sn atom occupying in between 1st and 2nd layer surrounded by six sulfur atoms with D_{3d} symmetry. DFT band structures calculated along (c) M–Γ–M and (d) K–K.

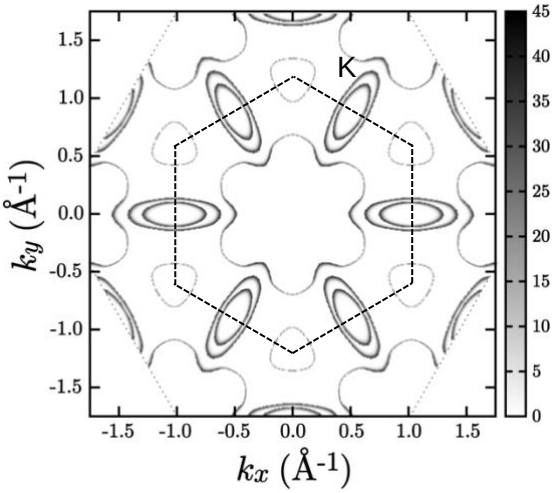

Figure 6. DFT electronic band structure at the Fermi energy for the Sn-intercalated 1T-TiS_2(0001) slab model.